http://www.aimspress.com/journal/Materials

Research article

Influences of vacancy defects on tensile failure of open-tip carbon nanocones

Ming-Liang Liao *

Department of Aircraft Engineering, Air Force Institute of Technology, Kaohsiung 820, Taiwan

* Correspondence: Email: minsliao@gmail.com.

Abstract：This paper studied influences of vacancy defects on tensile failure of open-tip carbon nanocones (CNCs) by molecular dynamics simulations. Carbon nanocones, perfect and containing mono-vacancy defects (including CNCs with the upper-vacancy, the middle-vacancy, and the lower-vacancy), were simulated in order to understand the influence of the presence and location of the vacancy defects on the CNCs tensile behavior. Some findings were obtained. It was found that the upper-vacancy CNC has the greatest degradation in the failure strain and the failure load among the three vacancy-defect CNCs, and the lower-vacancy CNC has the smallest degradation in the failure strain and the failure load. Degradation in the failure load is larger than degradation in the failure strain. Moreover, no apparent yielding (large elongation) was observed before failure of the studied CNCs. All the vacancy-defect CNCs were broken near the top end rather than near the vacancy location of the CNCs. The behaviors of the vacancy-location-dependent degradation and the vacancy-location-independent failure (namely, the near top-end failure) of the vacancy-defect CNCs are quite different from those of vacancy-defect CNTs (carbon nanotubes). These particular behaviors are ascribed to non-uniform diameters along the cone axes of the CNCs.

Keywords: tensile behavior; failure modes; failure strains; vacancy defects; molecular dynamics

1. Introduction

Similar to carbon nanotubes (CNTs), carbon nanocones (CNCs) also have many extraordinary

and distinguished properties. As a result, in recent years, researchers have taken great interests in discovering the properties and potential applications of CNCs as well as the related carbon nanomaterilas [1]. Regarding the initial research on CNCs, Ge and Sattler [2] found that there are five types of CNCs each having a particular apex angle. Later, Krishnan et al. [3] confirmed the existence of the five types of CNCs and demonstrated that they have apex angles of 19.2°, 38.9°, 60°, 84.6°, and 112.9°, respectively. Iijima et al. [4] proposed a production technique for carbon nanohorns (CNHs), which are sometimes also known as CNCs. Structures, production, properties, and applications of CNHs and CNCs were reviewed by Yudasaka et al. [5]. Naess et al. [6] observed wall structures and morphologies of the five types of CNCs by transmission electron microscopy, synchrotron X-ray, and electron diffraction. Like CNTs, CNCs can also be categorized as single-walled and multi-walled CNCs (SWCNCs and MWCNCs) according to the number of layers in the CNCs [7,8]. Mass growth of CNC arrays can be obtained by plasma-assisted approaches [9,10]. Besides, open-tip CNCs (with their tips truncated) could be produced [11,12] under appropriate control of synthetic conditions. The open-tip CNCs were proved having the same apex angles and structures to their closed-tip counterparts [13]. Recently, Karousis et al. [14] also made a review on structure, properties, functionalization, and applications of CNHs.

In recent years, researchers have utilized the special cone-shape structure of CNCs to discover practical applications of CNCs. For example, CNCs are very suitable for scanning probe tips [15,16], electron field emitters [17], and nanoindentation [18], since their tips can provide high resolution and large intensity. Moreover, because of their favorable feature for hydrogen adsorption [19,20], CNCs could also be used to develop hydrogen-storage materials. Owing to these encouraging applications, researchers have taken considerable interests in studying mechanical behaviors of CNCs. For example, Jordan and Crespi [21] investigated mechanical chiral inversion of CNCs compressed by a spherical indenter on their tips with the aid of molecular dynamics (MD) simulations. Tsai and Fang [22] studied the nucleation, thermal stability, and nanomechanics of CNCs. Liew et al. [23] examined buckling and post-buckling behaviors of open-tip CNCs having an apex angle of 19.2°. They also inspected mechanical properties of the CNCs under tensile loads [24]. In recent years, Liao et al. [25] investigated tensile and compressive behaviors of open-tip CNCs under axial strains. Fakhrabadi et al. studied elastic as well as buckling properties [26] and mechanical characterization [27] of CNCs by the methods of molecular mechanics and molecular dynamics, respectively. Yan et al. [28] examined buckling behaviors of CNCs having different apex angles by means of a mesh-free computational framework. They also studied bending buckling behaviors of CNCs having an apex angle of 19.2° by a quasi-continuum approach [29]. Besides, Liao [30] explored buckling behaviors of open-tip CNCs under elevated temperature conditions. Recently, Gandomani et al. [31] examined dynamic stability, including natural frequencies and natural modes, of SWCNCs conveying fluid. Wang et al. [32] used a temperature-related multiscale quasi-continuum model to investigate finite deformation of SWCNCs under axial compression.

Although there are substantial accomplishments in investigating mechanical behaviors of CNCs, studies on mechanical behaviors of CNCs containing defects (such as vacancy defects) are rare. With increasing practical applications of CNCs, this issue becomes significant in recent years. Similar to CNTs, defects can appear in CNCs at the stage of their growth or purification process [33] as well as during their device production. Defects can also be created deliberately to achieve desired

functionalities by chemical treatments or irradiation [34]. As a result, it is worthy of examining influences of defects on mechanical behaviors of CNCs.

For completeness, research works on mechanical behaviors of CNTs containing defects are surveyed briefly. For example, Sammalkorpi et al. [35] investigated mechanical properties of CNTs with vacancies and related defects. Haskins et al. [36] inspected the role of mono-vacancy defects on elastic moduli and tensile failure of SWCNTs. Sun and Liew [37] investigated fracture evolution of SWCNTs containing a vacancy defect. Hao et al. [38] employed molecular dynamics simulations to study axial compressive buckling of defective SWCNTs and MWCNTs. Poelma et al. [39] explored influences of the position of single vacancy defect on compressive stability of CNTs. Eftekhair et al. [40] examined effects of defects on the local shell buckling and post-buckling behaviors of SWCNTs and MWCNTs. Sharma et al. [41] inspected effects of Stone-Wales and vacancy defects on elastic moduli of CNTs and their composites. Recently, Sakharova et al. [42] have studied elastic properties of SWCNTs containing vacancy defects.

Contrary to the significant achievements in investigating mechanical behaviors of CNTs containing defects, studies on this topic for CNCs are not many in available literature. Regarding this topic, Liao [43] investigated influences of vacancy defects on buckling behaviors of open-tip CNCs. To give more information on this topic for the practical applications of CNCs, this paper expanded the author's previous study [43] to explore influences of vacancy defects on tensile failure of open-tip CNCs. Effects of temperature and vacancy location on the tensile failure were investigated in this paper. Modelling and numerical simulation of this study are described in the following section.

2. Modelling and Numerical Simulation of SWCNC's Tensile Behavior

Molecular dynamics (MD) simulations were used in this study to investigate influences of vacancy defects on tensile failure of open-tip CNCs. The Tersoff bond-order potential [44,45], which was successfully used for modeling of the mechanical behavior of CNC structures [18,22,25,30,43], was also employed in the current study. The Tersoff bond-order potential can be written as [44,45]

$$U = \sum_{i} \sum_{j>i} U_{ij},$$ (1)

in which U is the potential energy of the CNC system; U_{ij} is the bond energy between atoms i and j, which can be expressed as

$$U_{ij} = f_c(r_{ij})[U_R(r_{ij}) + b_{ij}U_A(r_{ij})],$$ (2)

where $U_R(r_{ij})$ and $U_A(r_{ij})$ are, respectively, the repulsive energy and the attractive energy between atoms i and j, $f_c(r_{ij})$ represents a smooth cutoff function, and r_{ij} is the distance between atoms i and j. The function b_{ij} stands for the bond order for atoms i and j. Expressions for the above functions and the corresponding parameters can be obtained from the reference [45].

The reason for choosing the Tersoff bond-order potential in this study is its computational efficiency for investigating tensile behaviors of carbon nanomaterials. It is noteworthy that, in recent

years, the second-generation reactive bond order (REBO) potential [46] or the adaptive intermolecular reactive bond order (AIREBO) potential [47] has been widely used in studies for mechanical behaviors of carbon nanomaterials. The second-generation REBO potential was proposed based on the Tersoff bond-order potential with special corrections to the bond order term for remedying the overbinding between atoms and for considering the dihedral angle for double bonds. The AIREBO potential is also based on the Tersoff bond-order potential with adaptive treatments of the dispersion, intermolecular repulsion, and torsional interactions. The long-range atomic interactions are also included in the AIREBO potential. Because of the modifications in the second-generation REBO potential and the AIREBO potential, both potentials could provide more accurate results than the Tersoff bond-order potential does, and are widely used in the studies for mechanical behaviors of CNTs and CNCs. Just owing to the modifications, both potentials are less computationally efficient than the Tersoff bond-order potential. Since tensile failure behaviors of open-tip CNCs were investigated in this study, it requires very large computation time for MD simulations of the study. Computation efficiency is also a significant concerned factor of this study. Considering computation efficiency of the simulations, the Tersoff bond-order potential, which was successfully employed in investigations into tensile behaviors of graphene [48], CNTs [49], and CNCs [25], was also selected for this study, though it offers less accurate results than the REBO potential or the AIREBO potential does.

Having the potential functions described above, interaction forces among carbon atoms in the CNC system can be determined from the gradient of the potential functions. Equations of motion for the CNC system can then be obtained. Evolution of each carbon atom could be attained by integrating the equations of motion. Behaviors of the CNC system subjected to tension can be examined accordingly. In this study, Gear's fifth predictor-corrector algorithm [50] with a time step of 1 fs (10^{-15} s) was employed for integrating the equations of motion. Besides, NVT (canonical) ensembles were employed during the simulations, and the velocity rescaling method [51] was utilized as a thermostat to keep the system at a specified temperature.

Before performing the MD simulations, a SWCNC model was constructed. In this study, the software Nanotube Modeler [52] was used for building of the SWCNC model. Figure 1 plots the SWCNC model of this study, where a SWCNC model for an open-tip SWCNC with an apex angle of 19.2°, a cone height of 40 Å, a top diameter of 8 Å, and a bottom diameter of 22 Å was built. In the model, the CNC was separated into three regions including moving, thermal, and fixed regions. Both the fixed (the bottom) and the moving (the top) regions have a height of a tenth (1/10) of the total height of the CNC. The fixed region was devised to model the fixture imposed on the CNC during applying axial tension. Atoms in the fixed region were completely restrained during the simulations. The moving region was designed to apply the axial tension on the CNC. In this paper, the axial tension was applied and controlled by an upward axial displacement of the moving region, which was set to move gradually at a very small and constant speed of 10 m/s. The thermal (the middle) region of the SWCNC model was used as a thermostat. Velocities of atoms in this region were adjusted via the velocity rescaling method to control the system temperature keeping at a specified temperature.
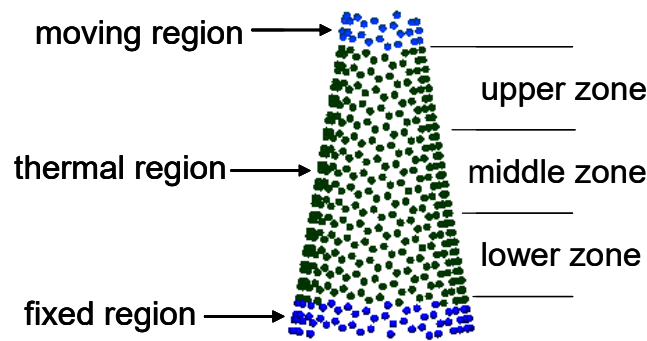
Figure 1. SWCNC model of the study.

For examining influences of vacancy location on tensile failure of the CNC, the middle region (namely, the strained region) was further divided into the upper, middle, and lower zones. Each zone has the same height. Moreover, a vacancy defect was arranged in the middle of the half front wall of each zone in order to discuss the influences of vacancy location. With this arrangement, an upper-vacancy CNC, a middle-vacancy CNC, and a lower-vacancy CNC were generated, as shown in Figure 2. It is noteworthy that each vacancy defect was created by removing an atom near the midway point rather than the centroid of the half front wall of each zone (as displayed in Figure 2) in order to examine influences of the height of the vacancy location. Beside, to discuss influences of vacancy defects on tensile failure of the CNC, a perfect model (without any vacancy defect) consisting of 770 carbon atoms and the three vacancy-defect models were analyzed. Since one atom was removed from the perfect CNC, the percentage of the removed atoms in each vacancy-defect CNC is 0.13%.
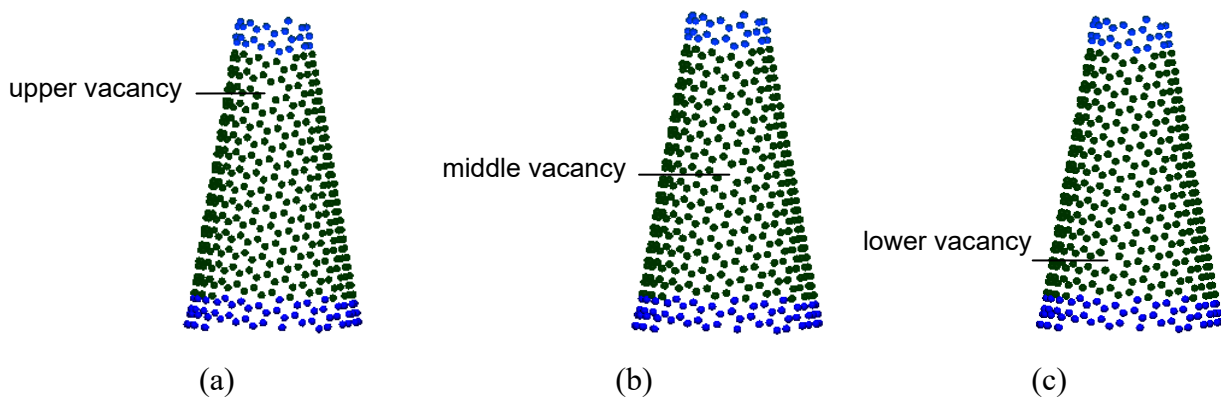

Figure 2. Locations of the vacancies in the investigated CNCs: (a) upper vacancy, (b) middle vacancy, and (c) lower vacancy. Only half of the atoms are plotted in order to show the vacancy location.

After constructing the three models for the vacancy-defect CNCs, the MD simulations were performed on the three models and also on the perfect model. Results of these models were compared to evaluate influences of vacancy defects on tensile failure of the CNCs. It should be noted that, to focus on influences of vacancy defects on tensile failure behaviors of the CNCs and to

simplify the problem, effects of posterior bond reconstruction were not examined in this study. It requires more detailed examination to discuss this issue. Nevertheless, the SWCNC models were subjected to structure relaxation before the MD simulations in order to eliminate artificial constraints established during construction of the SWCNC models and to obtain an initial structure with minimum potential energy. After the structure relaxation, constraints were imposed on the moving and the fixed regions. Then, axial tension was applied, and the MD simulations were carried out. Data during the simulations were analyzed to examine influences of vacancy defects on tensile failure of the CNCs.

3.   Results and Discussion

Influences of vacancy defects on tensile failure of open-tip CNCs were investigated in this study. Moreover, to understand influences of temperature on tensile failure of the vacancy-defect CNCs, three temperature conditions of 100, 300, and 500 K were considered in the study. Figure 3 plots the axial tensile force versus the axial tensile strain for the perfect and the vacancy-defect CNCs at 300 K. For each CNC, the tensile force was found growing with the tensile strain up to a specific strain (namely, the failure strain) after which the tensile force had a sudden drop, and tensile failure of the CNC occurred. The failure strains of the perfect, upper-vacancy, middle-vacancy, and lower-vacancy CNCs are 24.2, 23.6, 23.9, and 24.0%, respectively. The corresponding failure loads are 245, 234, 243, and 244 nN, respectively.
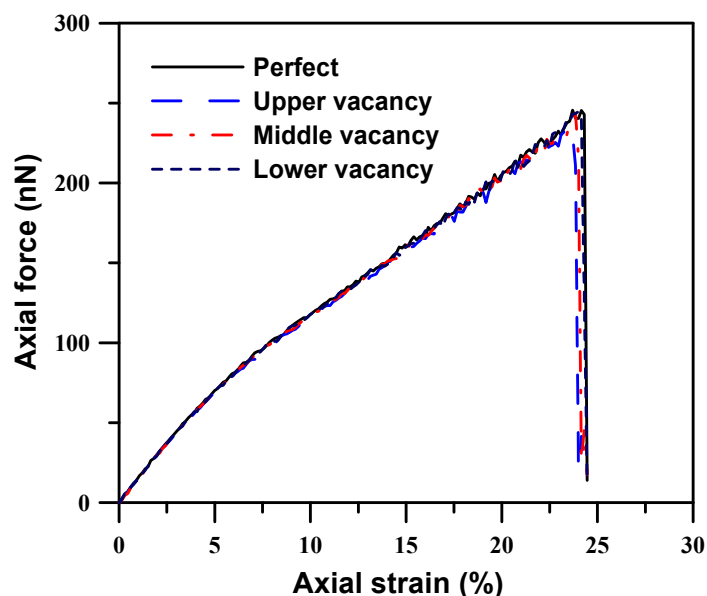

Figure 3. Axial force versus axial strain for the perfect and the vacancy-defect CNCs at 300 K.

To discuss temperature effects on tensile failure of the vacancy-defect CNCs, Figure 4 displays the axial tensile force versus the axial tensile strain for the middle-vacancy CNC at the three temperatures. The failure strain and the failure load were found to decrease with growing temperature. The decrease is ascribed to larger kinetic energy of the CNC at a higher temperature.

The larger kinetic energy caused the CNC easily to be broken at the higher temperature. As the temperature grew, apparent oscillation was also observed in the curves for the tensile force. The apparent oscillation in these curves results from the larger kinetic energy and the greater oscillating motion of the CNC at a higher temperature. Similar behaviors were also found in this study for the perfect and the other two vacancy-defect CNCs. These behaviors could also be observed in the studies for compressive buckling of open-tip CNCs [30,43].
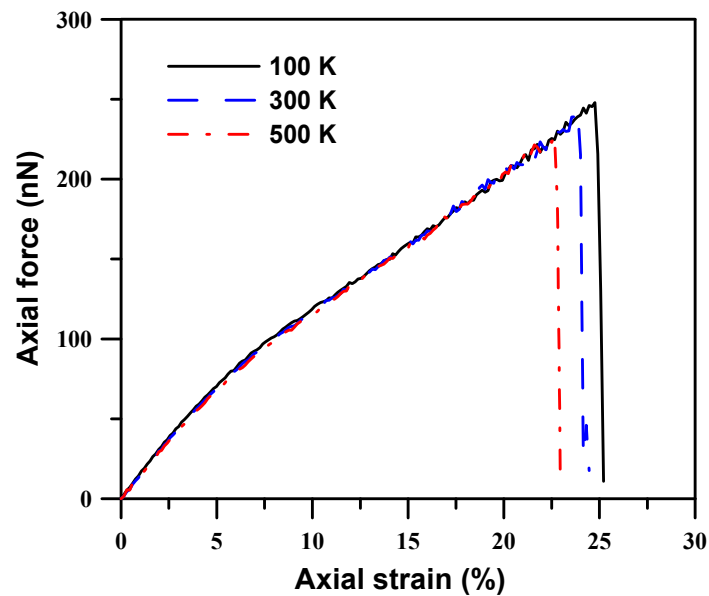

Figure 4. Axial force versus axial strain for the middle-vacancy CNC at the three temperatures.
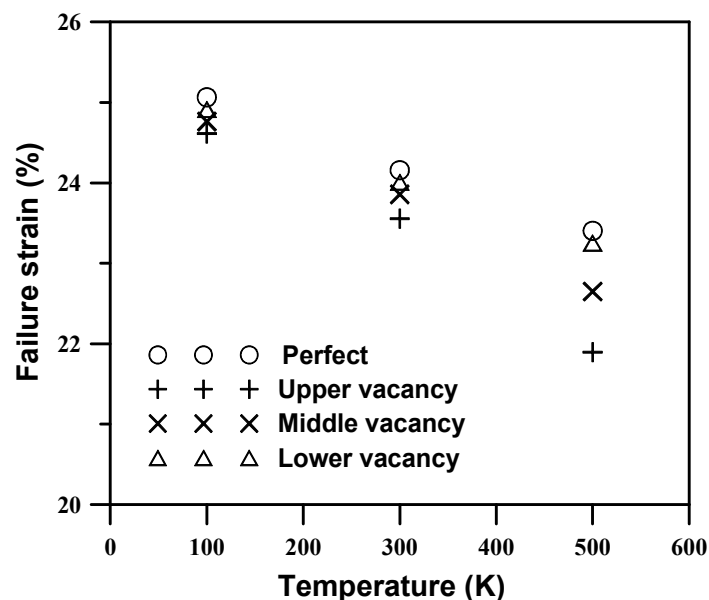

Figure 5. Failure strain of the perfect and the vacancy-defect CNCs at the three temperatures.

Figures 5 and 6 plot the failure strain and the failure load, respectively, of the perfect and the

vacancy-defect CNCs at the three temperatures. The temperature effects discussed above could also be observed from the figures. It was also found that the upper-vacancy CNC has the smallest failure strain and the smallest failure load, and the lower-vacancy CNC has a larger failure strain and a larger failure load than the middle-vacancy CNC does. The decrease in the failure strain and the failure load of the vacancy-defect CNCs with respect to those of the perfect CNC is more evident for the upper-vacancy CNC. Namely, the upper-vacancy CNC has the greatest degradation (with respect to the perfect CNC) in the failure strain and the failure load, and the lower-vacancy CNC has the lowest degradation in the failure strain and the failure load. The vacancy-defect CNCs have vacancy-location-dependent degradation in the failure properties (the failure strain and the failure load). That is, the degree of degradation (decrease) in the failure properties of vacancy-defect CNCs is dependent on the location of the vacancy defect rather than independent of the vacancy location.
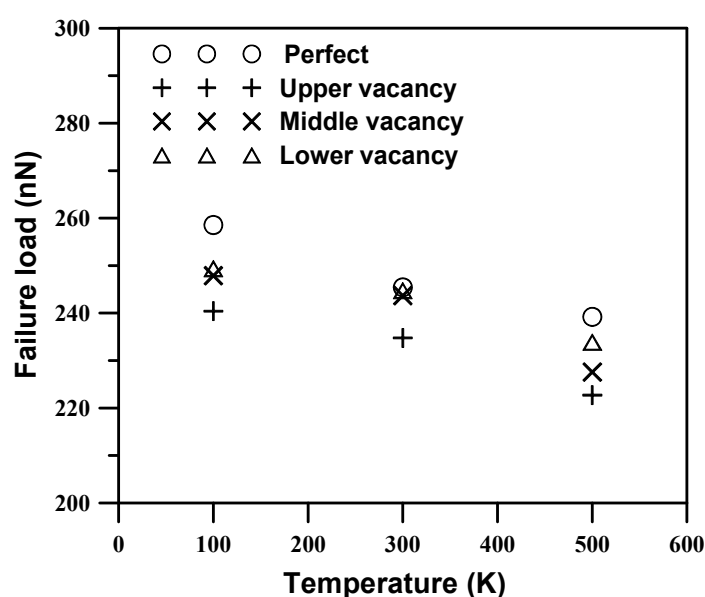

Figure 6. Failure load of the perfect and the vacancy-defect CNCs at the three temperatures.

The vacancy-location-dependent degradation behavior of the vacancy-defect CNCs results from non-uniform diameters along the cone axes of the CNCs. Since the upper zone has smaller cross-section areas because it has smaller diameters, the CNC with a vacancy in the upper zone (i.e., the upper-vacancy CNC) has a larger fraction of vacancies of 0.65% (the ratio of the number of vacancies to the number of atoms in the zone) as compared with 0.40% for the CNC with a vacancy in the lower zone (i.e., the lower-vacancy CNC), when just considering the specific zone in which the vacancy exists. The upper-vacancy CNC thus is much easily to be broken when subjected to axial tension, as compared with the other two vacancy-defect CNC. The upper-vacancy CNC hence has the greatest degradation in the failure strain and the failure load among the three vacancy-defect CNCs. Under the same reasoning, the lower-vacancy CNC has the smallest degradation in the failure strain and the failure load. Similar behaviors could also be observed for the studied cases at temperatures of 100 and 500 K.

The above observations show that the vacancy-defect CNCs have vacancy-location-dependent

degradation in tensile failure properties. This vacancy-location-dependent degradation behavior is quite different from the vacancy-location-independent degradation behavior of vacancy-defect CNTs. Their elastic properties and tensile failure properties are independent of the location of the vacancy defect [35,41,42]. Nevertheless, it should be noted that the critical buckling strain and the critical buckling load of CNTs were found to be significantly influenced by the vacancy location at very low temperature. However, the influences are small at room temperature [39].

It is worthy to note that, from Figures 5 and 6, degradation in the failure load of the vacancy-defect CNCs is larger than degradation in the failure strain. This feature could also be observed in compressive buckling of open-tip CNCs with vacancy defects [43], where degradation in the critical load of the vacancy-defect CNCs was found to be greater than degradation in the critical strain. For ease of comparison between influences of vacancy defects on tensile failure and on compressive buckling of open-tip CNCs, several typical results from a previous study of the author are also shown in this paper. In the study [43], influences of mono-vacancy defects on compressive buckling behaviors of open-tip CNCs were investigated. The CNCs considered in the study are the same as those analyzed in this paper. Figure 7 displays the critical strain and the critical load of the perfect and the middle-vacancy CNCs at the three studied temperatures. From the figure, the critical load/critical strain degradation feature discussed above could be observed. Buckling mode morphologies for the perfect and the vacancy-defect CNCs could be found in the study [43].
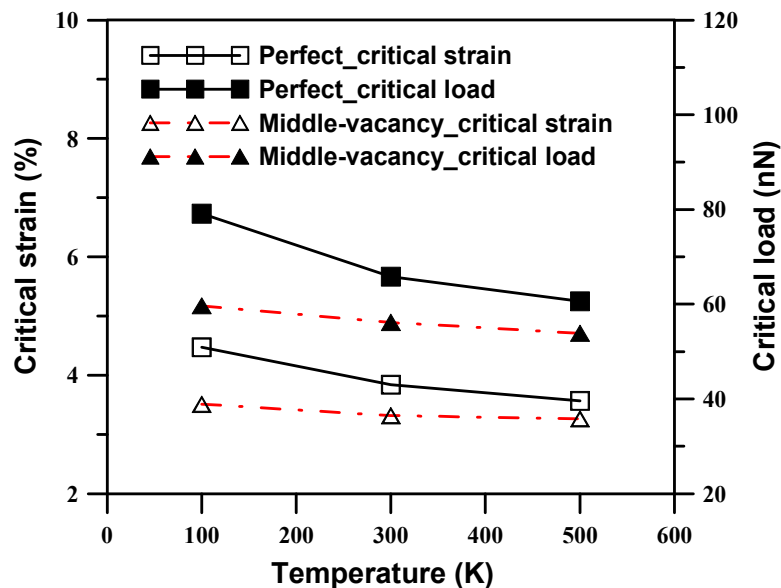

Figure 7. Critical strain and critical load of the perfect and the middle-vacancy CNCs at the three temperatures [43].

Comparing results of the current study (Figures 5 and 6) with those of the compressive buckling study (Figure 7), different degradation behaviors with respect to temperature growth could be found. As opposed to compressive buckling behaviors of the vacancy-defect CNCs, the tendency that the degree of degradation in antibuckling ability of the CNCs decreases with growing temperature (referring to Figure 7) was not observed in the current tensile loading cases (referring to Figures 5

and 6). The degree of degradation in the failure strain and the failure load did not decrease as the temperature grew.

Figure 8 displays morphologies near failure of the middle-vacancy CNC at 300 K. The corresponding tensile strains at which the morphologies were taken are shown in the caption of the figure. No obvious yielding (large elongation) was observed before failure of the CNC. The CNC was broken near the top end rather than near the vacancy location (the middle) of the CNC. The near top-end failure behavior is also owing to the non-uniform diameters along the cone axis of the CNC. With this geometry, the region near the top end has smaller cross-section area and thus has a higher stress than the other regions. The CNC therefore was broken near the top (the narrowest) end, though there has a vacancy in the middle zone of the CNC. The break occurring near the top end rather than just at the top end is due to thermal oscillation of the cone body caused by the system temperature. The near top-end failure was also found in the other cases of this study, including the perfect, the upper-vacancy, and the lower-vacancy CNCs. It was also found at the other two temperatures (100 and 500 K). This vacancy-location-independent failure behavior (namely, the near top-end failure) is different from the tensile failure behaviors of CNTs containing a vacancy [36,37]. Bond failure was found to spread from the vacancy defect of the CNTs, and then the bonds around the vacancy failed. Consequently, it caused entire failure of the CNTs.
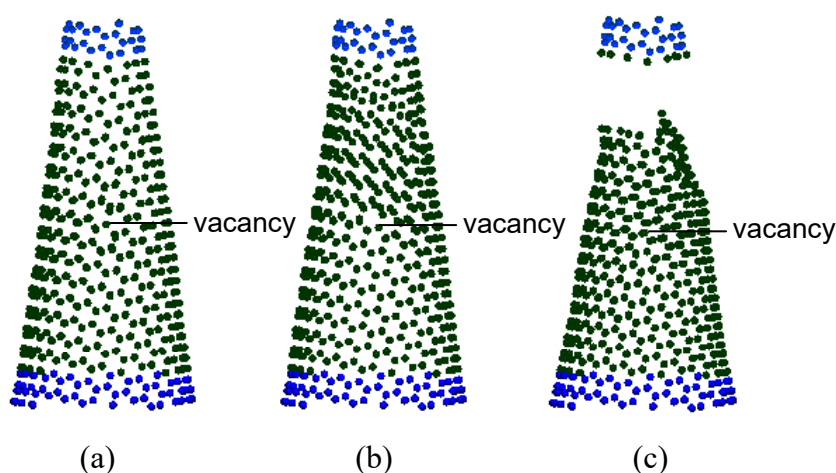

(a)   (b)   (c)

Figure 8. Morphologies near failure of the middle-vacancy CNC at 300 K: (a) before the failure strain (at 23.8%), (b) at the failure strain (at 23.9%), and (c) after the failure strain (at 24.2%). The atom at the vacancy location is the atom in the back wall of the CNC.

From the above observation, one can see that all the studied CNCs display a brittle failure mode. There was no apparent yielding (large elongation) before failure of the CNCs. The brittle failure mode could also be found in the open-tip CNCs investigated by Wei et al. [24]. It also occurred in CNCs pulled under the conditions of a much slower pulling rate and a higher temperature. This can be seen from a previous study of the author [25]. In the study, several CNCs having an apex angle of 19.2° and various cone heights were pulled at a much slower pulling rate of 0.1 m/s (as compared with   10 m/s of the current study) and at various temperatures. Results of the study show that all the examined CNCs exhibit a brittle failure mode, even for the highest CNC (with cone height of 60 Å)

at the higher temperature of 500 K. The cone height, temperature, and a much slower pulling rate seem to have no evident influences on the brittle failure mode of the CNCs.

As opposed to the brittle failure mode of the studied CNCs, CNTs could exhibit a brittle failure mode or a ductile failure mode depending on their external conditions and their tube symmetry. All CNTs are brittle at high strain and low temperature conditions, while armchair CNTs can be completely or partially ductile at low strain and high temperature conditions [53].

It is worthy to investigate the influences of removing an atom from the rear rather than from the front wall of the studied CNCs. The influences of a double vacancy defect (for example, by removing two atoms from the front wall) on tensile failure behaviors of the open-tip CNC are also a worthy research issue. To investigate the above issues, another middle-vacancy CNC (named the rear-wall middle-vacancy CNC for ease of discussion) and a double-vacancy CNC were also examined in this study. The rear-wall middle-vacancy was designed by removing an atom from the rear wall of the CNC. The removed atom has nearly the same relative position as that of the previously studied middle-vacancy CNC (named the front-wall middle-vacancy CNC), which contains middle-vacancy defect in the front wall of the CNC. The double-vacancy CNC was formed by removing two atoms from the front wall of the CNC. The two removed atoms are just selected as the atoms locating, respectively, at the upper vacancy and at the middle vacancy of this study (as shown in Figure 2).
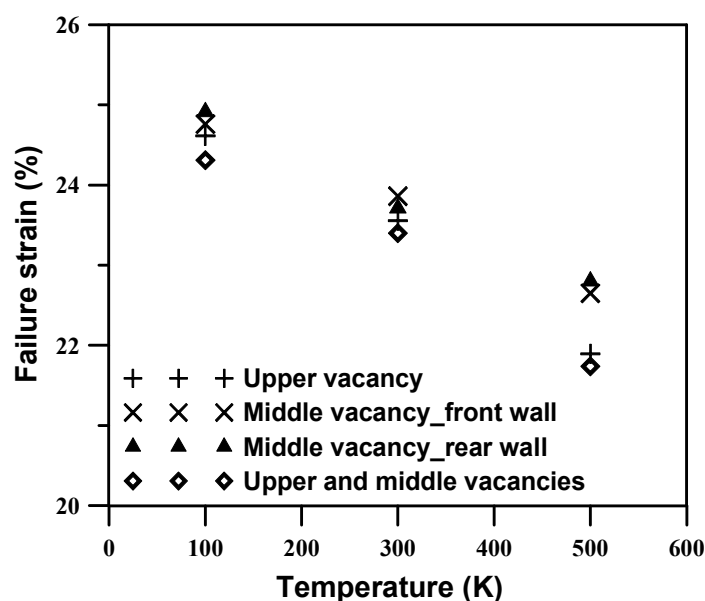

Figure 9. Comparisons of the failure strain for the middle-vacancy and the double-vacancy CNCs at the three temperatures.

Figures 9 and 10 show the failure strain and the failure load, respectively, of the rear-wall middle-vacancy CNC and the double-vacancy CNC. Results of the front-wall middle-vacancy CNC and the upper-vacancy CNC are also appended in both figures for comparison purposes. From the figures, it was found that the difference between results of removing an atom from the rear middle zone and those from the front middle zone is not evident. The failure strain and the failure load of the

rear-wall middle-vacancy CNC are near those of the front-wall middle-vacancy CNC. Removing an atom from the rear middle zone has nearly the same influences as removing an atom from the front middle zone.
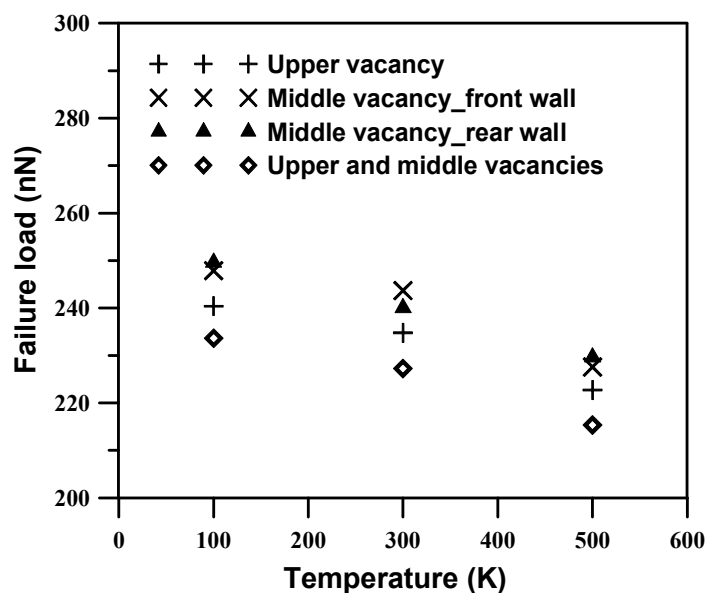

Figure 10. Comparisons of the failure load for the middle-vacancy and the double-vacancy CNCs at the three temperatures.

Comparing results of the double-vacancy CNC with those of the upper-vacancy CNC, it was found that the double-vacancy CNC has less failure strain and failure load than the upper-vacancy CNC does. However, the decrease in both failure properties is not large. From morphologies near failure of the double-vacancy CNC, the near top-end failure discussed above was also observed in the double-vacancy CNC. Owing to the near top-end failure, slight decrease in the failure properties was found in the double-vacancy CNC. Further investigations are required to understand influences of multiple-vacancy defects on tensile failure behaviors of the open-tip CNC.

4.   Conclusion

In this study, influences of vacancy defects on tensile failure of open-tip CNCs have been examined by the molecular dynamics simulations. Effects of vacancy location and temperature were inspected in the study. For ease of discussion, a perfect and three vacancy-defect CNCs (including the upper-vacancy, the middle-vacancy, and the lower-vacancy CNCs) were examined, and their results were compared to attain influences of vacancy defects on tensile failure of the CNCs.

From results of the study, it was found that the upper-vacancy CNC has the largest degradation in the failure strain and the failure load among the three vacancy-defect CNCs, and the lower-vacancy CNC has the smallest degradation in the failure strain and the failure load. Namely, the vacancy-defect CNCs have vacancy-location-dependent degradation in the failure properties. It was also observed that degradation in the failure load of the vacancy-defect CNCs is greater than

degradation in the failure strain. In addition, the failure strain and the failure load of the studied CNCs were found to decrease with growing temperature. Regarding the failure morphologies of the vacancy-defect CNCs, no apparent yielding (large elongation) was observed before failure of the CNCs. The CNCs were broken near the top end rather than near the vacancy location of the CNCs. Non-uniform diameters along the cone axes of the CNCs are responsible for the vacancy-location-dependent degradation and the vacancy-location-independent failure (namely, the near top-end failure) of the vacancy-defect CNCs. These particular behaviors are quite different from those of vacancy-defect CNTs.

Although the CNCs with mono-vacancy defects and, for comparison purposes, an open-tip CNC with a double vacancy were considered in this study, influences of multiple-vacancy defects (more than double vacancy) on tensile failure of open-tip CNCs might be deduced qualitatively from the results of the double-vacancy CNC. Quantitative investigations into the influences need more detailed studies. This issue and influences of the corresponding removed-atom fraction on tensile failure of the vacancy-defect CNCs are valuable works for the future study of the author.

Since investigations into the topic of the present study are rare in available literature, the present research might provide some information about influences of vacancy defects on tensile failure of open-tip CNCs. This information is helpful for practical applications of the CNCs, such as designs of nanodevices using the CNCs.

Acknowledgements

Conflict of Interest

The author declares that there is no conflict of interest regarding the publication of this paper.

References

1. Tagmatarchis N (2012) *Advances in Carbon Nanomaterials: Science and Applications*, Singapore: Pan Stanford Publishing.
2. Ge M, Sattler K (1994) Observation of fullerene cones. *Chem Phys Lett* 220: 192–196.
3. Krishnan A, Dujardin E, Treacy MMJ, et al. (1997) Graphitic cones and the nucleation of curved carbon surfaces. *Nature* 388: 451–454.
4. Iijima S, Yudasaka M, Yamada R, et al. (1999) Nanoaggregates of single-walled graphitic carbon nanohorns. *Chem Phys Lett* 309: 165–170.
5. Yudasaka M, Iijima S, Crespi VH (2008) Single-wall carbon nanohorns and nanocones. *Top Appl Phys* 111: 605–629.
6. Naess SN, Elgsaeter A, Helgesen G, et al. (2009) Carbon nanocones: wall structure and morphology. *Sci Technol Adv Mater* 10: 065002.
7. Gogotsi Y, Dimovski S, Libera JA (2002) Conical crystals of graphite. *Carbon* 40: 2263–2267.

8. Zhang G, Jiang X, Wang E (2003) Tubular graphite cones. *Science* 300: 472–474.

9. Tsakadze ZL, Levchenko I, Ostrikov K, et al. (2007) Plasma-assisted self-organized growth of uniform carbon nanocone arrays. *Carbon* 45: 2022–2030.

10. Levchenko I, Ostrikov K, Long JD, et al. (2007) Plasma-assisted self-sharpening of platelet-structured single-crystalline carbon nanocones. *Appl Phys Lett* 91: 113115.

11. Terrones H, Hayashi T, Muñoz-Navia M, et al. (2001) Graphitic cones in palladium catalysed carbon nanofibers. *Chem Phys Lett* 343: 241–250.

12. Endo M, Kim YA, Hayashi T, et al. (2002) Structural characterization of cup-stacked-type nanofibers with an entirely hollow core. *Appl Phys Lett* 80: 1267.

13. Ekşioğlu B, Nadarajah A (2006) Structural analysis of conical carbon nanofibers. *Carbon* 44: 360–373.

14. Karousis N, Suarez-Martinez I, Ewels CP, et al. (2016) Structure, properties, functionalization, and applications of carbon nanohorns. *Chem Rev* 116: 4850–4883.

15. Chen IC, Chen LH, Gapin A, et al. (2008) Iron-platinum-coated carbon nanocone probes on tipless cantilevers for high resolution magnetic force imaging. *Nanotechnology* 19: 075501.

16. Sripirom J, Noor S, Koehler U, et al. (2011) Easily made and handled carbon nanocones for scanning tunneling microscopy and electroanalysis. *Carbon* 49: 2402–2412.

17. Yu SS, Zheng WT (2010) Effect of N/B doping on the electronic and field emission properties for carbon nanotubes, carbon nanocones, and graphene nanoribbons. *Nanoscale* 2: 1069–1082.

18. Hsieh JY, Chen C, Chen JL, et al. (2009) The nanoindentation of a copper substrate by single-walled carbon nanocone tips: a molecular dynamics study. *Nanotechnology* 20: 095709.

19. Adisa OO, Cox BJ, Hill JM (2011) Open Carbon Nanocones as Candidates for Gas Storage. *J Chem Phys C* 115: 24528–24533.

20. Liao ML (2012) A study on hydrogen adsorption behaviors of open-tip carbon nanocones. *J Nanopart Res* 14: 837.

21. Jordan SP, Crespi VH (2004) Theory of carbon nanocones: mechanical chiral inversion of a micron-scale three-dimensional object. *Phys Rev Lett* 93: 255504.

22. Tsai PC, Fang TH (2007) A molecular dynamics study of the nucleation, thermal stability and nanomechanics of carbon nanocones. *Nanotechnology* 18: 105702.

23. Liew KM, Wei JX, He XQ (2007) Carbon nanocones under compression: buckling and post-buckling behaviors. *Phys Rev B* 75: 195435.

24. Wei JX, Liew KM, He XQ (2007) Mechanical properties of carbon nanocones. *Appl Phys Lett* 91: 261906.

25. Liao ML, Cheng CH, Lin YP (2011) Tensile and compressive behaviors of open-tip carbon nanocones under axial strains. *J Mater Res* 26: 1577–1584.

26. Fakhrabadi MMS, Khani N, Omidvar R, et al. (2012) Investigation of elastic and buckling properties of carbon nanocones using molecular mechanics approach. *Comput Mater Sci* 61: 248–256.

27. Fakhrabadi MMS, Dadashzadeh B, Norouzifard V, et al. (2013) Application of molecular dynamics in mechanical characterization of carbon nanocones. *J Comput Theor Nanos* 10: 1921–1927.

28. Yan JW, Liew KM, He LH (2012) A mesh-free computational framework for predicting buckling behaviors of single-walled carbon nanocones under axial compression based on the moving Kriging interpolation. *Comput Method Appl M* 247: 103–112.

29. Yan JW, Liew KM, He LH (2013) Buckling and post-buckling of single-wall carbon nanocones upon bending. *Compos Struct* 106: 793–798.

30. Liao ML (2014) Buckling behaviors of open-tip carbon nanocones at elevated temperatures. *Appl Phys A* 117: 1109–1118.

31. Gandomani MG, Noorian MA, Haddadpour H, et al. (2016) Dynamic stability analysis of single walled carbon nanocone conveying fluid. *Comput Mater Sci* 113: 123–132.

32. Wang X, Wang J, Guo X (2016) Finite deformation of single-walled carbon nanocones under axial compression using a temperature-related multiscale quasi-continuum model. *Comput Mater Sci* 114: 244–253.

33. Andrews R, Jacques D, Qian D, et al. (2001) Purification and structural annealing of multiwalled carbon nanotubes at graphitization temperatures. *Carbon* 39: 1681–1687.

34. Ni B, Sinnott SB (2000) Chemical functionalization of carbon nanotubes through energetic radical collisions. *Phys Rev B* 61: R16343.

35. Sammalkorpi M, Krasheninnikov A, Kuronen A, et al. (2004) Mechanical properties of carbon nanotubes with vacancies and related defects. *Phys Rev B* 70: 245416.

36. Haskins RW, Maier RS, Ebeling RM, et al. (2007) Tight-binding molecular dynamics study of the role of defects on carbon nanotube moduli and failure. *J Chem Phys* 127: 074708.

37. Sun Y, Liew KM (2008) Application of the higher-order Cauchy-Born rule in mesh-free continuum and multiscale simulation of carbon nanotubes. *Int J Numer Meth Eng* 75: 1238–1258.

38. Hao X, Qiang H, Xiaohu Y (2008) Buckling of defective single-walled and double-walled carbon nanotubes under axial compression by molecular dynamics simulation. *Compos Sci Technol* 68: 1809–1814.

39. Poelma RH, Sadeghian H, Koh S, et al. (2004) Effects of single vacancy defect position on the stability of carbon nanotubes. *Microelectron Reliab* 52: 1279–1284.

40. Eftekhari M, Mohammadi S, Khoei AR (2013) Effect of defects on the local shell buckling and post-buckling behavior of single and multi-walled carbon nanotubes. *Comput Mater Sci* 79: 736–744.

41. Sharma S, Chandra R, Kumar P, et al. (2014) Effect of Stone-Wales and vacancy defects on elastic moduli of carbon nanotubes and their composites using molecular dynamics simulation. *Comput Mater Sci* 86: 1–8.

42. Sakharova NA, Pereira AFG, Antunes JM, et al. (2016) Numerical simulation study of the elastic properties of single-walled carbon nanotubes containing vacancy defects. *Compos Part B-Eng* 89: 155–168.

43. Liao ML (2015) Influences of vacancy defects on buckling behaviors of open-tip carbon nanocones. *J Mater Res* 30: 896–903.

44. Tersoff J (1986) New empirical model for the structural properties of silicon. *Phys Rev Lett* 56: 632–635.

45. Tersoff J (1989) Modeling solid-state chemistry: interatomic potentials for multi-component systems. *Phys Rev B* 39: 5566–5568.

46. Brenner DW, Shenderova OA, Harrison JA, et al. (2002) A second-generation reactive empirical bond order (REBO) potential energy expression for hydrocarbons. *J Phys-Condens Mat* 14: 783–802.

47. Stuart SJ, Tutein AB, Harrison JA (2000) A reactive potential for hydrocarbons with intermolecular interactions. *J Chem Phys* 112: 6472–6486.

48. Mortazavi B, Remond Y, Ahzi S, et al. (2012) Thickness and chirality effects on tensile behavior of few-layer graphene by molecular dynamics simulations. *Comput Mater Sci* 53: 298–302.

49. Hwang CC, Wang YC, Kuo QY, et al. (2010) Molecular dynamics study of multi-walled carbon nanotubes under uniaxial loading. *Physica E* 42: 775–778.

50. Rapaport DC (2004) *The Art of Molecular Dynamics Simulations*, Cambridge: Cambridge University Press.

51. Haile JM (1997) *Molecular Dynamics Simulation: Elementary Method*, New York: John Wiley & Sons.

52. Nanotube Modeler, JCrystalSoft, 2016. Available from: http://jcrystal.com/products/wincnt/index.htm.

53. Nardelli MB, Yakobson BI, Bernholc J (1998) Brittle and Ductile Behavior in Carbon Nanotubes. *Phys Rev Lett* 81: 4656–4659.